Reversible electric-field manipulation of the adsorption morphology and magnetic anisotropy of small Fe and Co clusters on graphene

M. Tanveer,[1] J. Dorantes-Dávila,[2] and G. M. Pastor[3]
[1]*Institut für Theoretische Physik, Universität Kassel, 34132 Kassel, Germany*
[2]*Instituto de Física, Universidad Autónoma de San Luis Potosí, 78000 San Luis Potosí, Mexico*
[3]*Institut für Theoretische Physik, Universität Kassel, 34132 Kassel, Germany*
(Received 7 February 2017; revised manuscript received 23 October 2017; published 8 December 2017)

First-principles electronic calculations show how the adsorption morphology, orbital magnetism, and magnetic anisotropy energy (MAE) of small Co_N and Fe_N clusters ($N \leqslant 3$) on graphene (G) can be reversibly controlled under the action of an external electric field (EF). A variety of cluster-specific and EF-induced effects are revealed, including (i) perpendicular or canted adsorption configurations of the dimers and trimers, (ii) significant morphology-dependent permanent dipole moments and electric susceptibilities, (iii) EF-induced reversible transitions among the different metastable adsorption morphologies of Fe_3 and Co_3 on graphene, (iv) qualitative changes in the MAE landscape driven by structural changes, (v) colossal values of the magnetic anisotropy $\Delta E \simeq 45$ meV per atom in Co_2/G, (vi) EF-induced spin-reorientation transitions in Co_3/G, and (vii) reversibly tunable coercive field and blocking temperatures, which in some cases allow a barrierless magnetization reversal of the cluster. These remarkable electric and magnetic fingerprints open new possibilities of characterizing and exploiting the size- and structural-dependent properties of magnetic nanostructures at surfaces.

DOI: 10.1103/PhysRevB.96.224413

I. INTRODUCTION

Small clusters of 3*d* transition-metal (TM) clusters constitute one of the most challenging subjects in fundamental and applied nanostructure research. They show remarkable size- and structural-dependent physical behaviors, and they are potentially crucial components in the development of novel materials for high-density storage media, medical applications, and spin-electronic devices, for example [1–7]. One of the properties of central interest in this context is the magnetic anisotropy energy (MAE), which determines the low-temperature orientation of the magnetization with respect to the structure of the system, as well as its stability against temperature- and quantum-induced fluctuations. Together with the local moments and exchange interactions, the MAE conditions the magnetization dynamics under the action of external magnetic fields. It is therefore central to most applications, including high-performance storage and recording. In past years, 3*d* TM clusters deposited on highly polarizable 4*d* and 5*d* surfaces [8–10] as well as nanoscale alloys involving 3*d*, 4*d*, and 5*d* TMs [11,12] have attracted considerable attention. Indeed, the strong spin-orbit coupling at the 4*d* and 5*d* elements, combined with the spin polarization induced by the hybridization with 3*d* TMs, has been shown to offer new possibilities of enhancing and tuning the MAE. However, 3*d* adatoms on metallic surfaces show short spin lifetimes due to electron-electron scattering, which could reduce the stability of the magnetization, even if the MAE is large [13,14]. In this context, graphene (G) appears to be a promising alternative substrate. In this case, large spin-lifetimes are obtained, which should favor a stable magnetization [15]. Moreover, the singular electronic structure of the hexagonal C layer, with its linear dispersion relation, is expected to reveal novel magnetic behaviors [5,16]. Consequently, 3*d* TM clusters on graphene are not only remarkably interesting from a fundamental perspective, but they could also become the building blocks of new devices for specific applications.

In past years, broad and intense research activity has been devoted to understanding how the magnetic behavior of nanostructures can be tailored by manipulating the fundamental sample parameters, such as lattice structure and growth conditions, substrate composition, overlayer capping, alloy formation by codeposition, etc. [17–43]. While these investigations regularly open new directions in quantum material design, the interest in controlling the sample magnetization by using external sources such as spin-polarized currents, laser fields, and static electric fields (EFs) has also been growing steadily [28–43]. In particular, the use of EFs appears to be a promising alternative method of steering the spin degrees of freedom, particularly since it should be both reversible and energetically competitive [41]. Recent experiments have actually shown that an external EF can modify the magneto-anisotropic behavior of metal-oxide semiconductors [44–50], thin films [51–54], nanocomposite thin films [55], and nanomagnets [40]. Moreover, an EF-induced magnetization reversal has been achieved by modifying the interface exchange bias in multiferroic laminates [39]. It has also been demonstrated that the magnetization direction of a nanomagnet can be manipulated by means of the EF generated by the tip of a scanning tunneling microscope [40]. Finally, theoretical studies performed in the context of single-molecules, multilayers, and surface nanostructures have shown that nanoscale magnetism can be very sensitive to external EFs [31,33–37].

In many applications, for example in magnetic storage and memory devices, not only does one seek large anisotropy energies, and therefore particularly stable magnetizations, but one is equally interested in finding tunable, fast, and efficient mechanisms to reverse the magnetization in the writing processes [40,41]. Standard reversal techniques using an external magnetic field are often impractical due to the smallness of the nanoscale moments. Spin-polarized currents become inefficient due to the important resistive and dissipative side effects. In addition, the quest for bit miniaturization requires

large blocking temperatures and therefore large anisotropy energy barriers [40]. Achieving the corresponding large magnetic-field densities required for magnetization reversal in a selectively localized region is currently a serious challenge. Macroscopic EFs could be remarkably helpful in this context, provided that the magnetic material is designed to allow a significant reduction of the anisotropy barriers by switching on an appropriate EF when a spin reversal is intended. Removing the EF after the writing process would then restore the full MAE, thus avoiding a superparamagnetic loss of information [22]. In this way, both low power consumption and a fast magnetization reversal process could be achieved [40,41].

From the point of view of fundamental research, and in particular of theory, the challenge is to achieve a detailed quantum-mechanical understanding of the electric-field dependence of the magnetic behavior of TM nanostructures. This should provide the basis for the development of new materials that are susceptible to reversible EF control of the magnetization. Toward that end, we focus in this work on the adsorption morphology, magnetic anisotropy, and orbital magnetism of small Fe and Co clusters on graphene. In the following, we demonstrate the extent to which an external EF can be used to modify and control the most relevant nanostructures of fundamental and practical interest. Remarkable magnetoelectric fingerprints are thus revealed, which open up new possibilities of characterizing and exploiting the size- and structural-dependent properties of magnetic nanostructures at surfaces.

II. COMPUTATIONAL DETAILS

Electronic calculations on small Fe and Co clusters deposited on graphene have been performed by using the Vienna *ab initio* simulation package (VASP), which implements Hohenberg-Kohn-Sham's density-functional theory on a periodic supercell by allowing fully self-consistent relaxations of the atomic positions [56]. VASP solves the spin-polarized Kohn-Sham equations in an augmented plane-wave basis set, which incorporates the effects of core electrons on the valence states by means of the projector augmented wave (PAW) method [57]. The exchange and correlation contributions to the total energy functional have been taken into account by using Perdew-Wang's generalized-gradient approximation [58].

The plane-wave basis set considered in the calculations is characterized by the cutoff energy $E_{\max} = 500$ eV. Larger values of $E_{\max}$ have been tested for representative examples in order to verify that this choice is sufficiently accurate. The supercells, which model the nanostructures, contain 4×4 unit cells of the graphene layer in the case of deposited monomers and 6×6 unit cells in the case of deposited dimers and trimers. The C atoms are located in the xy plane, taking advantage of the periodic boundary conditions along the x and y directions. The z coordinates of the TM adatoms are all positive. The size of the supercell along the z direction is 16 Å in order to avoid any spurious interactions between the periodic replicas of the two-dimensional (2D) nanostructures. The Brillouin zone integrations are performed on a $5 \times 5 \times 1$ ($9 \times 9 \times 1$) Monkhorst mesh for the 6×6 (4×4) supercells. Gaussian functions having a width $\sigma = 50$ meV are used in order to broaden the Kohn-Sham energy levels and thus improve convergence. Series of calculations have been performed by reducing σ systematically until the residual entropy contribution to the total energy is less than 1 meV per atom.

The structures are fully relaxed by applying the conjugate-gradient method until the forces on all the atoms are less than 10^{-2} eV/Å. The criterion for energy convergence has been set to 10^{-5} eV for the structural optimizations and to 10^{-7} eV for the calculation of magnetic anisotropy energies. Notice that the latter are derived from independent self-consistent calculations for each direction of the magnetization. Our test calculations and systematic previous studies [59–61] show that these technical parameters yield a sufficiently high accuracy for our purposes. Any numerical fluctuations should have no influence on our physical conclusions [62].

Finally, the graphene layer is placed close to the boundary of the supercell in the z direction, and the uniform dipole density generating the external electric field $\vec{\varepsilon} = \varepsilon_z \hat{z}$ is located about 8 Å away from the graphene layer. In this way, spurious interactions with the dipole layer are avoided. A positive value of ε_z means that the external EF is directed parallel to the z axis from the graphene layer toward the TM adcluster. In all cases, the structures are fully relaxed in the presence of the applied EFs.

III. RESULTS

In this section, we present and discuss our theoretical results for the structural, electronic, and magnetic properties of small Fe_N and Co_N clusters on graphene having $N \leqslant 3$ atoms. In particular, we quantify the possibilities of manipulating the geometrical conformation, the easy magnetization direction, and the anisotropy-energy barriers of the deposited clusters by applying an external electric field $\vec{\varepsilon} = \varepsilon_z \hat{z}$, which is perpendicular to the C layer.

A. Fe clusters on graphene

In the case of a single Fe atom, the most stable adsorption site is the hollow position at the center of a hexagon of graphene. In the absence of an external EF, the easy magnetization direction of Fe_1/G lies within the graphene layer, and the calculated off-plane MAE is relatively small: $\Delta E_{xz} = E_x - E_z = -1.1$ meV. These results are in qualitative agreement with previous calculations [63]. When ε_z is switched on, the adsorption position remains the hollow site, and only very small changes in the MAE are observed, of the order of 1–2 % for $|\varepsilon_z| \leqslant 0.75$ V/Å.

The adsorption morphology of the Fe dimer shows a remarkable dependence on the applied EF. In Fig. 1 the most stable geometries of Fe_2 on graphene are illustrated for representative values of ε_z. For $\varepsilon_z = 0$ we find that Fe_2 adopts a remarkable canted upright equilibrium configuration, in which the dimer bond forms an angle $\delta = 12^{\circ}$ with the surface normal (z axis). This is qualitatively in agreement with previous calculations [60,61]. The strictly perpendicular configuration ($\delta = 0$) is found to be unstable, which can be interpreted as a Jahn-Teller distortion. The bond length $d_{\mathrm{FeFe}} = 2.07$ Å is significantly reduced with respect to the solid, in qualitative agreement with the contraction found in free Fe_2. The location of the bottom Fe atom is somewhat displaced from the centered

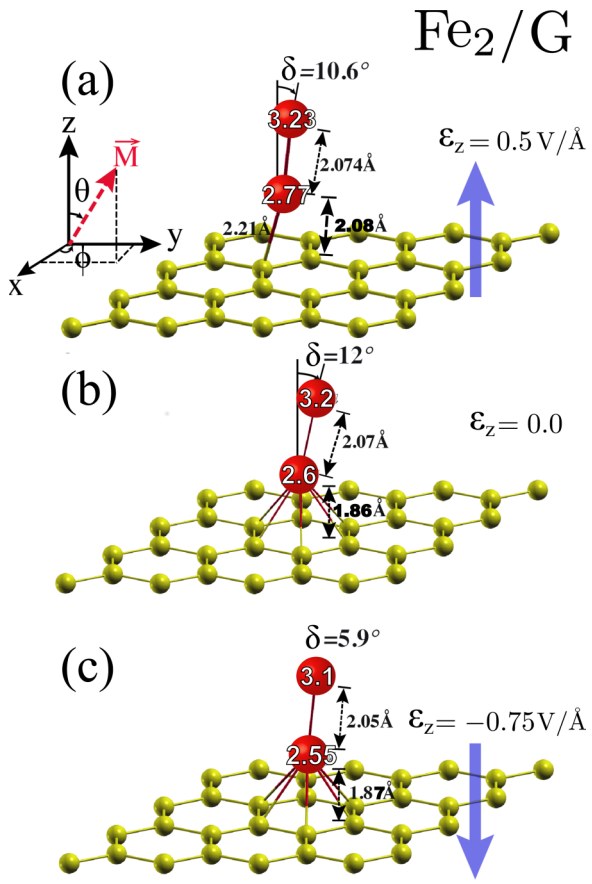

FIG. 1. Optimized structures of Fe_2 on graphene for representative values of the external electric field $\vec{\varepsilon} = \varepsilon_z \hat{z}$. The dimer adsorption position is toplike in (a), whereas it is hollowlike in (b) and (c). The corresponding calculated local spin moments μ_i, tilting angle δ, and bond lengths are indicated. In the inset of (a), the coordinate system is illustrated.

hollow position in the direction of a C–C bridge position. The actual displacement amounts to about 5% of the distance between the center of the hexagon and a C–C bond. For the sake of comparison, it is useful to point out that the distance between the bottom Fe atom and the plane defined by the graphene layer is $d_{\mathrm{FeG}} = 1.86$ Å [see Fig. 1(b)]. The local magnetic moments μ_i at the bottom atom ($i = 1$) and at the top atom ($i = 2$) are, as expected, much larger than in Fe bulk: $\mu_1 = 2.6\mu_{\mathrm{B}}$ and $\mu_2 = 3.2\mu_{\mathrm{B}}$. The significant difference between μ_1 and μ_2 reflects the effects of the hybridization of the d orbitals of the bottom Fe atom and the graphene layer. Similar results for the optimized structure and local spin moments have been reported in Ref. [61] for $\varepsilon_z = 0$.

The upright adsorption of Fe_2 on graphene defies the intuitive and most often valid idea of associating the strongest stability with the largest local coordination. It is therefore important to clarify its microscopic origin. For this purpose, we have repeated the adsorption geometry optimization in the nonmagnetic or paramagnetic (PM) case, i.e., by imposing a vanishing spin polarization. Remarkably, the most stable geometry of the Fe dimer in the nonmagnetic case is parallel to the C layer. In fact, the magnetic energy gained upon the development of magnetism in the optimal upright configuration ($\delta = 12^\circ$) is $\Delta E_{\mathrm{m}} = 145$ meV/at, which is clearly larger than the energy difference between the most stable upright and parallel geometries, which amounts to 45 meV/at. Note that the magnetic energy is given by $\Delta E_{\mathrm{m}} = E_{\mathrm{PM}} - E_{\mathrm{FM}}$, where E_{PM} and E_{FM} refer, respectively, to the paramagnetic and ferromagnetic solutions. One concludes that it is magnetism what stabilizes the unusual upright configuration. Identifying the central role played by the spin polarization on the ground-state energy as a function of adsorption configuration is a physical effect of fundamental interest. Moreover, it also provides a plausible physical explanation for the stability of the upright (low coordinated) geometries. It is in fact well known that a low local coordination of TM atoms favors the development of larger magnetic moments and higher exchange-energy gains, since it tends to narrow the width of the local density of $3d$ states. Reciprocally, magnetism often tends to stabilize structural arrangements with lower coordination numbers, where the exchange-energy gain is more important. As we shall see, similar trends are found for Fe_3, Co_2, and Co_3 on graphene. To our knowledge, the role of magnetism on the stability of the upright configurations found for magnetic TM dimers and trimers on graphene has never been discussed before. This may also provide a qualitative explanation for the trend to three-dimensional growth experimentally observed in small Fe islands on graphene [61].

The adsorption morphology and the magneto-anisotropic properties can be remarkably tuned by means of an external EF. For instance, for a perpendicular inward field $\varepsilon_z = -0.75$ V/Å (i.e., pointing from the cluster to the graphene layer), the dimer tends to align with the surface normal by reducing the angle between the bond and the z axis from $\delta = 12^{\mathrm{o}}$ to 5.9^{o}, while the dimer-layer distance $d_{\mathrm{FeG}} = 1.87$ Å remains almost the same as in the field-free case (see Fig. 1). This reorientation is driven by the coupling between the dipole moment $\vec{p}$ of Fe_2 and the EF, which tends to align $\vec{p}$ along $\vec{\varepsilon}$. In addition, we find that the spin moments are somewhat reduced to $\mu_1 = 2.55\mu_{\mathrm{B}}$ and $\mu_2 = 3.1\mu_{\mathrm{B}}$ [see Fig. 1(c)]. This indicates that the local exchange energy contributes to the stabilization of the larger tilting angles found for $\varepsilon_z = 0$. Furthermore, the orientation-dependent hybridizations between the Fe clusters and the graphene layer, which can be tuned to some extent with the EF, play an important role in the magnetic behavior of these nanostructures.

A qualitatively different behavior is found for outgoing EFs. For small ε_z, in the range $0 < \varepsilon_z < 0.45$ V/Å, no significant charge transfer between graphene and the Fe dimer occurs, and the hollow adsorption position remains quite robust. However, for $\varepsilon_z \geqslant 0.5$ V/Å, a drastic change in geometry is observed. The hollow position becomes unstable and the bottom Fe atom moves to a nearly top position above a C atom, as shown in Fig. 1(a). At the same time, the distance $d_{\mathrm{FeG}} = 2.08$ Å between the graphene layer and the bottom Fe atom is increased. The angle $\delta = 10.6^\circ$ between the dimer bond and the layer normal is also somewhat reduced, due to the coupling between $\vec{\varepsilon}$ and the induced electric dipole moment of Fe_2. These important structural modifications are in fact accompanied by significant field-induced redistributions of the local charges. Indeed, a charge transfer of $\Delta n \simeq -0.16$ electrons is observed for $\varepsilon = 0.5$ V/Å, mainly from the Fe dimer to the graphene layer. For comparison, the charge

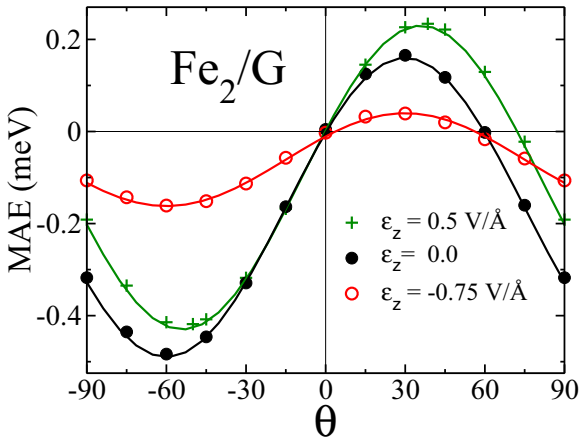

FIG. 2. Magnetic anisotropy energy $\Delta E = E(\theta) - E_z$ of Fe_2 deposited on graphene as a function of the polar angle θ between the magnetization $\vec{M}$ and the z axis. Representative values of the external field $\vec{\varepsilon} = \varepsilon_z \hat{z}$ are considered [see the inset of Fig. 1(a)]. Positive θ corresponds to the half-plane including the z axis and the dimer bond, while negative θ corresponds to the opposite half-plane, away from the dimer. The symbols show the actual self-consistent electronic results, while the curves are fits to those data using an $l = 2$ spherical harmonics expansion.

transfer induced by a strong inward field $\varepsilon_z = -0.75$ V/Å is $\Delta n = 0.09$ electrons, in this case from graphene to Fe_2. A further direct consequence of the change in the adsorption position found for $\varepsilon_z = 0.5$ V/Å is the enhancement of the local magnetic moment $\mu_1 = 2.77\mu_B$ at the bottom Fe atom. This can be ascribed to the reduction of the local Fe-C coordination number, as Fe_2 moves to the nearly top position, together with some increase in the number of d holes. As expected, the local moment $\mu_2 = 3.23\mu_B$ at the upper Fe atom is much less affected [see Fig. 1(a)]. These findings clearly demonstrate the remarkable possibilities of manipulating the structure and spin-polarized density distribution of small TM clusters on graphene by static electric means.

Unraveling the dependence of the magnetic anisotropy on the electric-field strength ε_z is probably the most important aspect of our investigations. In Fig. 2, the magnetic anisotropy energy $\Delta E = E(\theta) - E_z$ of Fe_2 on graphene is shown as a function of the polar angle θ between the magnetization $\vec{M}$ and the z axis for representative values of ε_z. The azimuthal angle $\phi = 0$ corresponds to the half-plane defined by the z axis and the tilted Fe_2, which is perpendicular to the graphene plane, passing through the center of a hexagon and the middle of a C–C bond. In the absence of an EF, the two opposite easy magnetization directions are $\hat{e}$, which has $\theta \simeq 60^\circ$ and $\phi = 180^\circ$ (away from the tilted bond), and $\hat{e}' = -\hat{e}$, which has $\theta \simeq 120^\circ$ and $\phi = 0$ (in the direction of tilting). This means that $\hat{e}$ and $\hat{e}'$ form an angle of about 72° with the dimer bond. The transition states for magnetization reversal $\hat{t}$ and $\hat{t}' = -\hat{t}$, being perpendicular to $\hat{e}$, are also tilted. Neither $\hat{e}$ nor $\hat{t}$ bears a simple geometrical relation to the Fe_2 bond or the layer normal. This is clearly a consequence of the very low symmetry of the adsorption configuration. Notice that $\Delta E(\theta)$ can be very accurately fitted by the second-order expansion in spherical harmonics: $\Delta E(\theta) \simeq \Delta E_b \sin^2(\theta - \theta_{\hat{e}})$, where $\Delta E_b = E(\hat{t}) - E(\hat{e})$ stands for the energy barrier involved in the magnetization reversal, and $\theta_{\hat{e}}$ refers to the easy axis (for example, $\theta_{\hat{e}} = 60^\circ$ for $\phi = 180^\circ$ in the field-free case). The quality of the fits, shown by the full curves in Fig. 2, might seem surprising taking into account that the electronic results (given by the symbols in Fig. 2) are obtained from independent self-consistent calculations for each orientation of $\vec{M}$. It shows, however, that in this case the second-order contributions of the spin-orbit interactions dominate the magnetization-direction dependence of the electronic energy, a not uncommon situation when the symmetry of the nanostructure is very low.

In the absence of an EF, the reversal barrier amounts to $\Delta E_b = 0.64$ meV. A positive, outward $\varepsilon_z = 0.5$ V/Å does not change the anisotropic behavior qualitatively. One observes a small shift of $\hat{e}$ toward the z axis, which now lies along $\theta \simeq 54^\circ$ and $\phi = 180^\circ$ ($\theta \simeq 126^\circ$ and $\phi = 0$ for $\hat{e}'$). This is probably related to the changes in the adsorption position. The transition state $\hat{t}$ remains perpendicular to $\hat{e}$ and is thus rotated accordingly. The energy barrier $\Delta E_b \simeq 0.66$ meV is almost the same as in the field-free case. A negative, inward $\varepsilon_z = -0.75$ V/Å does not change the position of the easy axis or the transition state significantly. However, the energy barrier $\Delta E_b = 0.20$ meV is reduced by more than a factor 3. This implies a similar reduction of the coercive field H_c and blocking temperature T_B, which could be used in order to trigger the magnetization reversal by switching on ε_z together with the external magnetic field. Removing subsequently ε_z, once $\vec{M}$ is flipped, would then stabilize the magnetization direction by restoring the original values of ΔE_b and T_B. An improved efficiency of the magnetic writing process is thus expected.

The Fe trimer shows several metastable adsorption configurations on graphene (i.e., local energy minima) whose relative stability changes as a function of the external field ε_z. These structures, labeled α, β, and γ, are illustrated in Fig. 3. The calculated field dependences of the corresponding electronic energies are shown in Fig. 4. One observes that for vanishing ε_z the slightly canted structure α is the most stable configuration of Fe_3 on graphene. This is in agreement with previous field-free calculations using similar methods [61]. Remarkably, one observes a transition to a different geometry β when an outward EF $\varepsilon_z \geqslant 0.2$ V/Å is applied. As illustrated in Fig. 3, this structural change involves a 60° rotation of the Fe_3 triangle around the axis, which goes through its center of gravity and is perpendicular to the triangle plane. While in the structure α atoms 2 and 3 are in direct contact with the graphene layer, in the structure β only atom 3 has C atoms in its immediate local environment. This implies a profound change in the cluster-substrate hybridization. The robustness of these adsorption geometries (local minima) has been confirmed by performing fully relaxed calculations in the whole range of ε_z.

The transition from the base-on-C configuration α to the vertex-on-C configuration β with increasing positive ε_z is consistent with the trends found for Fe_2 on graphene. In both cases, one observes that as $\varepsilon_z > 0$ increases, the deposited Fe cluster undergoes a drastic change from a well-coordinated vertical adsorption position to an arrangement in which the coordination to the C layer (i.e., the number of C atoms in the immediate environment of the Fe atoms) is minimal or particularly small. In contrast, for inward fields ($\varepsilon_z < 0$) no

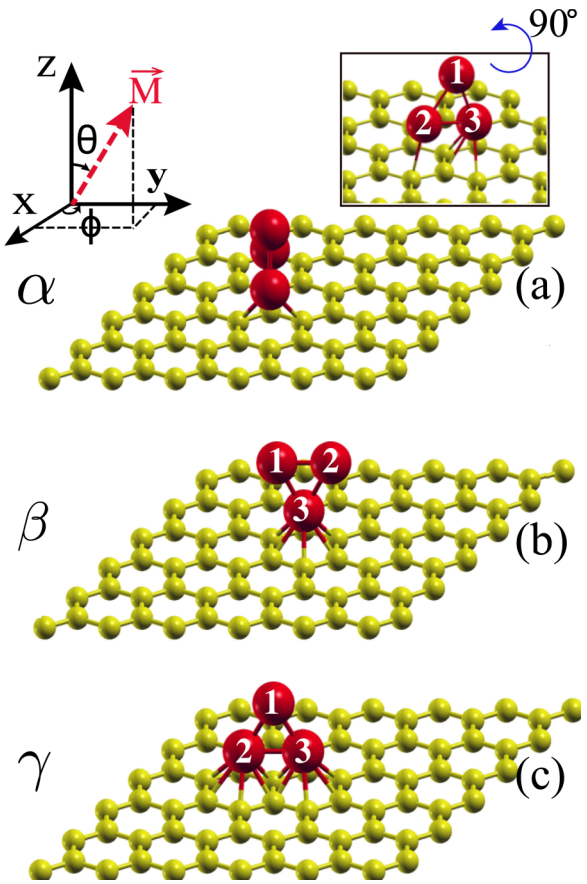

FIG. 3. Illustration of the different adsorption configurations α, β, and γ of Fe_3 and Co_3 on graphene. In (a) the coordinate system and a different perspective to the structure α are illustrated. Notice that in the optimized geometries, the trimer plane is perpendicular or nearly perpendicular to the graphene layer. In the structures α and γ, the basis of the triangle (atoms 2 and 3) is in contact with the graphene layer, while in β only atom 3 does.

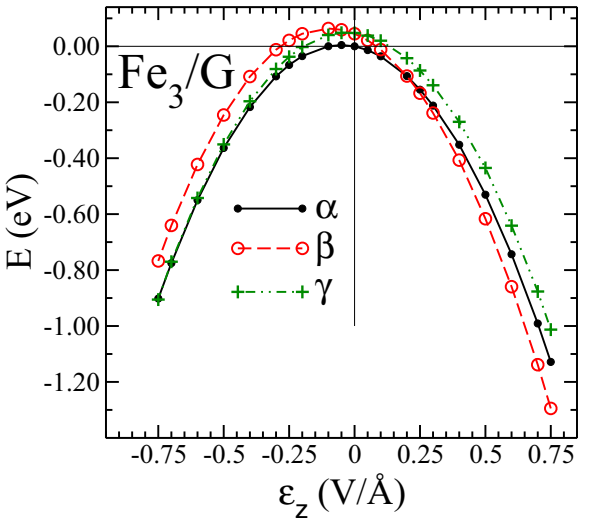

FIG. 4. Total energy E of Fe_3 on graphene as a function of the external electric field ε_z for the different optimized adsorption configurations α, β, and γ illustrated in Fig. 3.

such important structural changes are observed, at least in the considered range of $|\varepsilon_z|$. For $\varepsilon_z < 0$ one simply finds that the energy difference between the adsorption configurations α and γ tends to vanish as $|\varepsilon_z|$ increases ($|\varepsilon_z| \leqslant 0.75$ V/Å); see Fig. 4.

It is interesting to analyze the field dependence of the electronic energy $E = -p_0\varepsilon_z - \chi_e\varepsilon_z^2 + O(\varepsilon_z^3)$ as a function of ε_z in terms of the underlying permanent electric dipole moment p_0 and polarizability χ_e of the deposited cluster. From the *ab initio* results for $E(\varepsilon_z)$ shown in Fig. 4, one obtains $p_0 = 0.16$, 0.36, and 0.08 eV Å/V and $\chi_e = 1.80$, 1.91, and 1.79 eV $Å^2/V^2$ for the adsorption configurations α, β, and γ, respectively (see Fig. 3). Notice that the permanent dipoles are all positive and sizable, which is in line with the discussed electronic charge transfer from the deposited cluster to graphene. Moreover, the value of p_0 depends strongly on the adsorption configuration. Larger coordination numbers and stronger hybridizations with the C layer imply a stronger covalent character of the Fe_3-graphene bonding, which correlates with a weaker charge transfer and a smaller p_0. The electric polarizabilities are much less sensitive to the adsorption geometry. However, we do observe that χ_e is somewhat larger in the vertex-on-C configuration β.

We may now interpret the α-β structural transition from an electrostatic perspective. For $\varepsilon_z = 0$ the less coordinated β configuration is about $\Delta E_{\beta\alpha} = 0.05$ eV less stable than the α configuration. As a positive ε_z is applied, the structure developing the largest $p_0 > 0$ tends to be stabilized. A structural change occurs when the critical value $\varepsilon_z^c \simeq \Delta E_{\beta\alpha}/[p_0(\beta) - p_0(\alpha)] = 0.25$ V/Å is reached. For $\varepsilon_z < 0$ the trend is reversed. For ε_z the γ configuration is also less stable than the α configuration ($\Delta E_{\gamma\alpha} = 0.05$ eV). However, it shows a smaller p_0. Thus, as $|\varepsilon_z|$ increases ($\varepsilon_z < 0$) the energy difference between α and γ becomes smaller, until it nearly vanishes for $|\varepsilon_z| \simeq \Delta E_{\gamma\alpha}/[p_0(\alpha) - p_0(\gamma)] = 0.62$ V/Å.

In Table I, results are given for the magnetic properties of Fe_3 on graphene for representative values of the external electric field. One observes that for the most stable structures α and β the lowest-energy magnetization direction is always parallel to the graphene plane, irrespective of the considered ε_z (i.e., $\Delta E_{xz} < 0$ or $\Delta E_{yz} < 0$). Notice, moreover, that there is always a strong in-plane anisotropy $|\Delta E_{xy}| \simeq 0.9$-1.6 meV/at, which is often stronger than the usually considered off-plane anisotropies. The easy axis correlates with the adsorption configuration, namely $\hat{e} = \hat{x}$ for α and $\hat{e} = \hat{y}$ for β, but it happens to be independent of ε_z for a given structure, at least in the considered EF range. The same holds for the transition state $\hat{t}$ and hard axis $\hat{h}$, which are $\hat{t} = \hat{y}$ and $\hat{h} = \hat{z}$ ($\hat{t} = \hat{z}$ and $\hat{h} = \hat{x}$) for the configuration α (β). A strong field dependence of the magnetic anisotropy-energy landscape follows from the above discussed discontinuous change in the adsorption configuration. Indeed, the MAE landscape provides a remarkable fingerprint of the geometry of Fe_3 on graphene, which could thus be distinctively identified in experiment.

Quantitatively, the off-plane and in-plane anisotropy energies per atom are in the range $|\Delta E_{xz}| = 1.08-1.27$ meV for the α configuration and $|\Delta E_{yz}| = 0.91-1.53$ meV for the β

TABLE I. Magnetic properties of Fe_3 on graphene having the most stable adsorption configurations α and β shown in Fig. 3. Representative values of the external electric field $\vec{\varepsilon} = \varepsilon_z \hat{z}$ are considered, as indicated in V/Å. Results are given for the lowest-energy magnetization direction $\hat{e}$, the off-plane anisotropy energies per atom $\Delta E_{xz} = E_x - E_z$ and $\Delta E_{yz} = E_y - E_z$ (in meV), as well as the average orbital moments $\langle L \rangle_x$, $\langle L \rangle_y$, and $\langle L \rangle_z$ (in μ_B per atom), which are obtained when the magnetization $\vec{M}$ points along the x, y, and z axes, respectively (see Fig. 3).

Fe_3/G	ε_z	0.0	−0.75	0.75
	$\hat{e}$	x	x	x
	ΔE_{xz}	− 1.22	− 1.083	− 1.28
α	ΔE_{yz}	− 0.382	− 0.105	− 0.553
	$\langle L \rangle_x$	0.066	0.073	0.064
	$\langle L \rangle_y$	0.076	0.080	0.077
	$\langle L \rangle_z$	0.068	0.079	0.069
	$\hat{e}$	y	y	y
	ΔE_{xz}	0.265	0.104	0.485
β	ΔE_{yz}	− 1.077	− 1.53	− 0.916
	$\langle L \rangle_x$	0.077	0.080	0.075
	$\langle L \rangle_y$	0.065	0.075	0.060
	$\langle L \rangle_z$	0.060	0.065	0.060

configuration. The barrier energy involved in a magnetization reversal process increases for $\varepsilon_z = 0.75$ V/Å (outward EF) and decreases for $\varepsilon_z = -0.75$ V/Å (inward EF) by about 0.1–0.5 meV, as compared to the field-free case (see Table I). As in Fe_2 on graphene, this opens the possibility of using static external EFs in order to tune the transition rates in magnetization reversal processes.

Finally, concerning orbital magnetism, it is interesting to note that the magnetization direction yielding the largest orbital moment does not coincide with the easy axis (see Table I). A similar situation has often been found when, as in the present case, the orbital moments are small, particularly if the spin moments are not fully saturated [33,64]. This is due to the fact that the contribution of the diagonal part $L_z S_z$ of the spin-orbit energy is relatively small, and the majority spin $3d$ states do not lie well below the Fermi energy. Further details are given at the end of Sec. III B, where the densities of states (DOS) of Fe and Co trimers are contrasted.

B. Co clusters on graphene

The calculated most stable adsorption configuration of the Co atom is the hollow site for all values of ε_z. In the absence of an external EF, we obtain that the easy axis is perpendicular to the graphene layer along the z axis. The corresponding local spin and orbital moments within the Co Wigner-Seitz sphere amount to $\langle S_z \rangle = 1.11 \mu_B$ and $\langle L_z \rangle = 0.28 \mu_B$. The orbital-moment anisotropy $\Delta L_{zx} = 0.17 \mu_B$ is such that the largest $\langle L \rangle$ is developed along the easy axis, which is consistent with the predictions of perturbation theory [65]. The calculated $\Delta E_{xz} = 5.7$ meV is in qualitative agreement with the values $\Delta E_{xz} = 3.7$ meV reported in Ref. [37] and $\Delta E_{xz} = 1$ meV reported in Ref. [66]. However, it disagrees with Ref. [5], where $\Delta E_{xz} = -9.55$ meV was reported, thus implying an in-plane easy axis. Note that the latter result is close to the value $\Delta E_{xz} = -8.1 \pm 0.4$ meV inferred from scanning tunneling microscopy and spin-excitation spectroscopy on Co atoms deposited on graphene on a Pt (111) support [5] (see also the discussion below). The differences in ΔE_{xz} between the various density-functional calculations for the Co atom on free-standing graphene are most probably due to differences in the considered exchange and correlation functionals, and in the degree of the self-consistency required in the MAE calculations. For instance, in Ref. [5] the LDA+U approximation was used, while in Ref. [66] the GGA+U+J approximation was applied. This suggests that subtle electron correlation effects, for example quantum spin fluctuations, can play an important role in the magneto-anisotropic behavior of adatoms.

Contrasting our results for Co adatoms on graphene (G) with experiments helps to disclose the importance of the graphene-substrate hybridizations and of the modifications of the graphene electronic structure due to the coupling to its support. Recent measurements performed in the absence of an external EF have shown that the MAE of Co/G strongly depends on the choice of the metal substrate on which the graphene layer is deposited [19]. For instance, for Co atoms on G/Ru(0001), the easy magnetization direction is perpendicular to the C layer with $\Delta E_{xz} = 8.4 \pm 2.9$ meV. In contrast, the Co atom on G/Pt (111) shows an easy magnetization direction that is parallel to the graphene plane, with $\Delta E_{xz} = -8.1 \pm 0.4$ meV. In both cases, the orbital moments are relatively large, namely $\langle L \rangle = 1.71 \pm 0.16 \mu_B$ for G/Ru (0001) and $\langle L \rangle = 0.7 \mu_B$ for G/Pt (111). Moreover, when Co atoms are deposited on G/Ir (0001), the direction of the magnetization is perpendicular to the graphene layer and the orbital moment is strongly reduced ($\langle L \rangle = 0.09 \pm 0.02 \mu_B$). These substrate effects render a direct comparison between calculations for free-standing graphene layers and experiment rather hazardous. It would therefore be very interesting to theoretically quantify the role of the graphene support on the magnetic properties of deposited clusters.

In Fig. 5(a), results are shown for the off-plane MAE $\Delta E_{xz} = E_x - E_z$ of Co on graphene as a function of the electric field ε_z. As in previous cases, they were obtained as total energy differences by performing independent self-consistent calculations including spin-orbit interactions for each orientation of the magnetization $\vec{M}$. For all considered ε_z we find that $\Delta E_{xz} > 0$, which indicates that the easy axis is perpendicular to the graphene layer. In particular, for $\varepsilon_z = 0$ we have $\Delta E_{xz} = 5.6$ meV/at, a value about a factor 5 larger than the one found for the Fe monomer. In the inset of Fig. 5(a), the magnetic anisotropy energy $\Delta E(\theta) = E(\theta) - E_z$ is given as a function of the polar angle θ between $\vec{M}$ and the z axis. One observes that the MAE follows quite closely the second-order angular dependence $\Delta E(\theta) \simeq \Delta E_{xz} \sin^2 \theta$, which is characteristic of uniaxial behavior.

The value of ΔE_{xz} can be tuned to some extent by varying the external field, from $\Delta E_{xz} = 4.8$ meV for an outward field $\varepsilon_z = 0.75$ V/Å to $\Delta E_{xz} = 5.9$ meV/at for an inward field $\varepsilon_z = -0.5$ V/Å. Notice that according to our calculations, ΔE_{xz} remains positive in the whole considered EF range. This contrasts with the results obtained by using the force-theorem approximation and reported in Ref. [37], which show a strong decrease and a change of sign in ΔE_{xz} for large ε_z. These

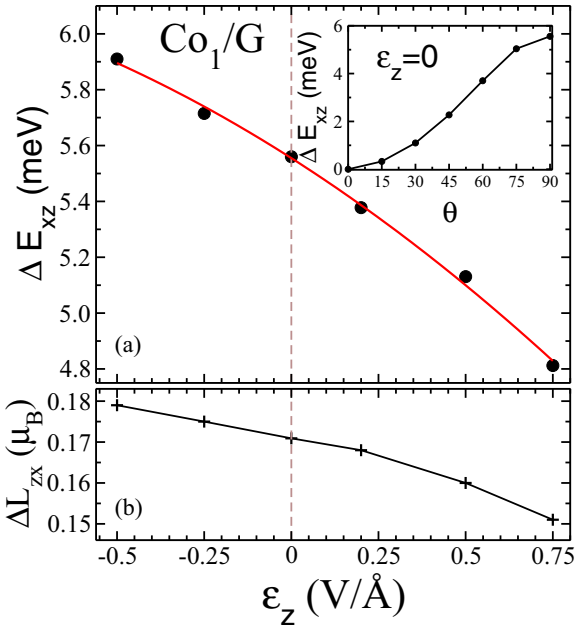

FIG. 5. Magnetic anisotropy energy $\Delta E_{xz} = E_x - E_z$ and orbital-moment anisotropy $\Delta L_{zx} = \langle L\rangle_z - \langle L\rangle_x$ of a Co atom on graphene as a function of the normal component ε_z of the electric field $\vec{\varepsilon} = \varepsilon_z \hat{z}$. Positive ε_z corresponds to $\vec{\varepsilon}$ pointing from the graphene layer toward the atom. The inset of (a) shows $\Delta E(\theta) = E(\theta) - E_z$ for $\varepsilon_z = 0$ as a function of the polar angle θ (in degrees) between $\vec{M}$ and the z axis.

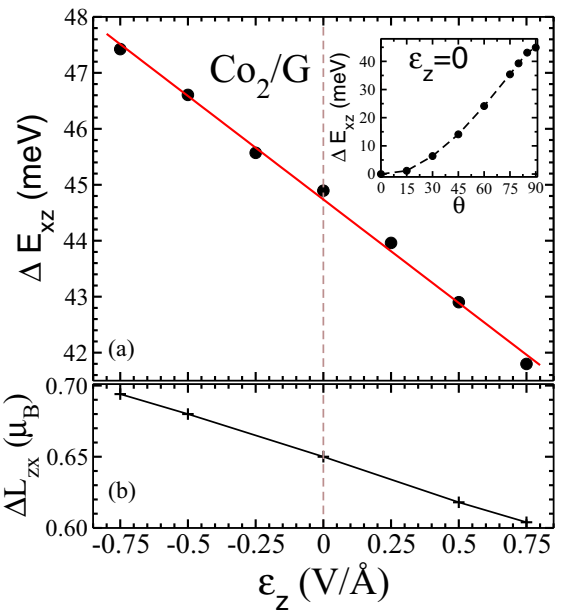

FIG. 6. Magnetic anisotropy energy per Co atom $\Delta E_{xz} = E_x - E_z$ and average Co orbital-moment anisotropy $\Delta L_{zx} = \langle L\rangle_z - \langle L\rangle_x$ of a Co dimer on graphene as a function of the normal component ε_z of the electric field $\vec{\varepsilon} = \varepsilon_z \hat{z}$. Positive ε_z corresponds to $\vec{\varepsilon}$ pointing from the graphene layer toward the dimer. In the inset of (a), the anisotropy energy $\Delta E(\theta) = E(\theta) - E_z$ is given for $\varepsilon_z = 0$ as a function of the polar angle θ between the magnetization $\vec{M}$ and the z axis.

qualitative differences between the two methods illustrate the importance of the redistributions of the spin and orbital polarized electronic density, as well as the resulting changes in the exchange-correlation potential in the presence of spin-orbit interactions. At least in this case they appear to be central to the magnetization-direction dependence of the ground-state energy. Comparison with Ref. [37] suggests that as the EF increases ($\varepsilon_z > 0$), the self-consistent treatment of spin-orbit interactions tends to increasingly stabilize the perpendicular magnetization direction relative to the in-plane direction, well beyond the predictions of the force-theorem approximation [67].

The orbital moment of the Co atom on graphene is in the range $\langle L\rangle = 0.27{-}0.30\mu_B$ depending on the magnetization direction and EF strength (see below). These values are significantly reduced with respect to the atomic one ($L = 3\mu_B$ for the $3d^8$ configuration according to Hund's rules), which reflects the importance of the symmetry breaking and interactions with the graphene layer. Still, $\langle L\rangle$ is significantly enhanced with respect to the fully coordinated Co-bulk environment ($\langle L\rangle_{\text{bulk}} = 0.13\mu_B$). To analyze the origin of the MAE and its dependence on the external EF, it is useful to consider the anisotropy $\Delta L_{zx} = \langle L\rangle_z - \langle L\rangle_x$ of the orbital magnetic moment, which is shown in Fig. 5(b) as a function of ε_z. First of all, one observes that ΔL_{zx} is positive. Thus, the system develops the largest orbital moment when $\vec{M}$ points along the easy axis. Moreover, ΔL_{zx} decreases with increasing ε_z, keeping an approximate proportionality relation between ΔE_{xz} and ΔL_{zx} (see Fig. 5). This is consistent with Bruno's second-order perturbation treatment of spin-orbit interactions [65]. From this perspective, the fact that $\Delta L_{xz} > 0$ even for a relatively large outward EF (e.g., $\varepsilon_z = 0.75$ V/Å) confirms the calculated stability of $\vec{M}$ along the easy z axis for large ε_z.

The most stable adsorption configuration of Co_2 on graphene is the hollow position, with the dimer bond perpendicular to the C layer. This contrasts profoundly with the behavior found for Fe_2, which shows a spontaneous symmetry breaking of the equilibrium position: Fe_2 is displaced from the center of the hexagon toward the middle of a C–C bond, and the dimer bond is tilted by about 12° away from the layer normal. It is interesting to note that the upright configuration of Co_2 on graphene is intimately related to its magnetic behavior. In fact, if one performs a paramagnetic (PM) calculation, one obtains, as already discussed for Fe_2, that the optimal adsorption geometry has the Co_2 bond lying parallel to the C layer. The magnetic energy gain is $\Delta E_m = E_{PM} - E_{FM} \simeq 130$ meV, whereas the energy difference between the upright and parallel magnetic configurations is only 35 meV/at. One concludes again that the upright configuration is driven by magnetism.

As shown in Fig. 6, the consequences of the highly symmetric equilibrium configuration of Co_2 could hardly be more striking, since the MAE and the orbital moments are remarkably large for a deposited TM dimer. For example, for $\varepsilon_z = 0$ we find $\Delta E_{xz} = 45$ meV and $\langle L\rangle_z = 0.8\mu_B$ per Co atom. These values are among the largest ones found in $3d$ TM nanostructures, even though the Co-Co and Co-C hybridizations are particularly strong. However, notice that $\langle L\rangle$ remains almost a factor 4 smaller than the atomiclike orbital moment observed for Co on MgO [17]. As for the Co atom, ΔE_{xz} and $\langle L\rangle_z$ are decreasing functions of ε_z. They can thus

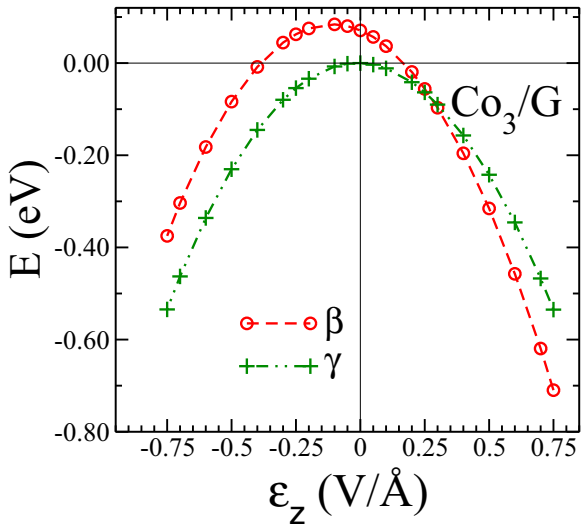

FIG. 7. Total energy of Co_3 on graphene (G) as a function of the external electric field ε_z for the optimized adsorption configurations β and γ illustrated in Fig. 3.

be tuned from $\Delta E_{xz} = 47.5$ meV/at and $\langle L\rangle_z = 0.84\mu_B$ for $\varepsilon_z = -0.75$ V/Å to $\Delta E_{xz} = 41.8$ meV/at and $\langle L\rangle_z = 0.75\,\mu_B$ for $\varepsilon_z = 0.75$ V/Å. In contrast, when $\vec{M}$ points along the $\hat{x}$ direction, the average orbital moments are strongly reduced, falling in the range $0.14 < \langle L\rangle_x < 0.15\mu_B$. Notice that the anisotropy of the average orbital moment ΔL_{zx} also decreases with increasing ε_z, following the behavior predicted by a second-order-perturbation treatment of spin-orbit interactions [65].

Figure 7 shows the electric-field dependence of the total energy of the optimized Co_3 structures β and γ, which are illustrated in Fig. 3. For an inward EF ($\varepsilon_z < 0$) and for $\varepsilon_z = 0$, the most stable adsorption configuration is γ, where Co_3 stands perpendicular to the graphene layer, and the base of the triangle is well coordinated to the C atoms [see Fig. 3(c)]. However, for an increasing outward field ($\varepsilon_z > 0$), the stability of this structure starts to decrease in comparison with the less-coordinated structure β. Finally, at $\varepsilon \simeq 0.25$ V/Å a transition to the structure β occurs. As in the case of Fe_3, this behavior can be interpreted in an electrostatic way by using the relation $E = -p_0\varepsilon_z - \chi_e\varepsilon_z^2 + O(\varepsilon_z^3)$ and comparing the zero-field permanent dipole moment p_0 and electric polarizability χ_e of the two structures. From the density-functional calculations, one obtains $p_0 = 0.225$ eV Å/V ($p_0 = 0.006$ eV Å/V) and $\chi_e = 1.01$ eV Å^2/V^2 ($\chi_e = 0.95$ eV Å^2/V^2) for the structure β (γ). Notice that both p_0 and χ_e are smaller in Co_3 than in Fe_3, which is consistent with the fact that the charge transfer between Co_3 and the C layer is smaller than for the Fe_3 cluster. The structural change occurring in Co_3 for $\varepsilon_z \simeq 0.25$ V/Å (see Fig. 7) has a similar origin to that observed in Fe_3. For a vanishing or weak external EF, the TM-C hybridization and bonding dominate. The structure γ, which has the largest coordination with the C layer, is the most stable [$\Delta E_{\beta\gamma} = E(\beta) - E(\gamma) = 0.07$ eV for $\varepsilon_z = 0$]. The charge transfer and the permanent dipole moment p_0 are small here. In contrast, the structure β, having a much weaker coordination with the C layer and a center of gravity located farther apart

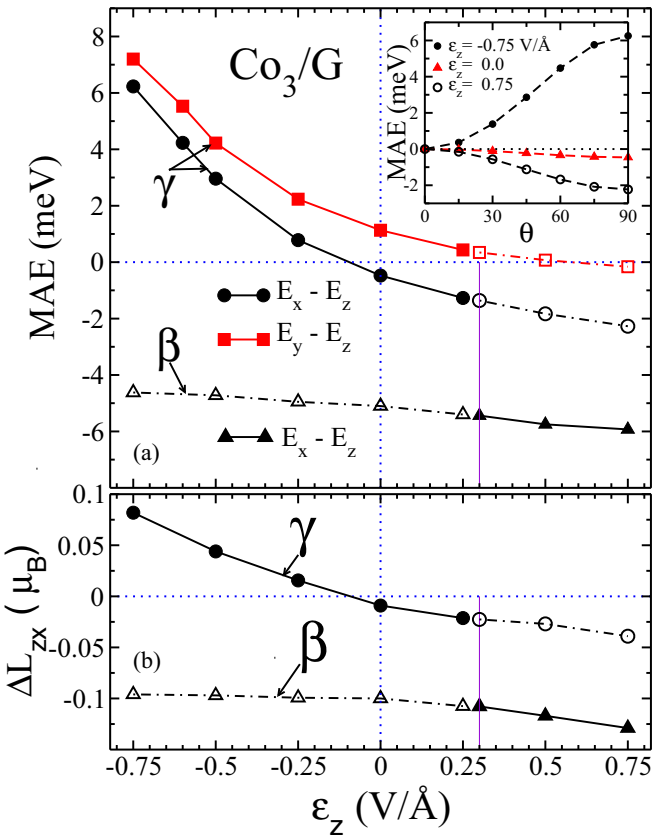

FIG. 8. Magnetic anisotropy energy and orbital-moment anisotropy of the most stable adsorption configurations of Co_3 on graphene as a function of the external electric field ε_z ($\vec{\varepsilon} = \varepsilon_z\hat{z}$). In (a) results are shown for $\Delta E_{xz} = E_x - E_z$ in the configurations β and γ, as well as for ΔE_{yz} in the configuration γ. Full symbols highlight the most stable adsorption morphology (see Figs. 3 and 7). In (b) the EF dependence of the average orbital-moment anisotropy $\Delta L_{zx} = \langle L\rangle_z - \langle L\rangle_x$ is shown. As in (a), solid lines and full symbols (dashed lines and open symbols) refer to the most stable (second best) structure. The inset in (a) shows the MAE $\Delta E(\theta) = E(\theta) - E_z$ as a function of the polar angle θ between $\vec{M}$ and the z axis for representative values of ε_z. The adsorption geometries and the coordinate system are illustrated in Fig. 3.

from it, develops an almost 40 times larger p_0. Thus, as the EF increases, β is rapidly stabilized with respect to γ, so that for $\varepsilon_z > \Delta E_{\beta\gamma}/[p_0(\beta) - p_0(\gamma)] \simeq 0.25$ V/Å it becomes the ground state.

In Fig. 8, results are given for the MAE of Co_3 on graphene in its most stable adsorption configurations β and γ as a function of ε_z (see also Fig. 3). For the structure β (vertex down) we find $\Delta E_{xz} \simeq -5$ meV/at, which implies that the easy axis is parallel to the graphene plane. In this case, the changes in ΔE_{xz} induced by the EF are relatively weak, of the order of 1 meV/at in the range $|\varepsilon_z| \leqslant 0.75$ eV/Å. They do not affect either the easy axis or the magnetization reversal barrier of this structure in a significant way. In contrast, in the configuration γ (vertex up) the MAE of Co_3 depends much more strongly on the EF, thus having a qualitative impact on the magnetic behavior. For $\varepsilon_z = 0$ the easy axis is parallel to the C plane, and the transition state $\hat{t}$ involved in a magnetization

reversal points along the layer normal z. The in-plane anisotropy energy $\Delta E_{yx} = 1.7$ meV/at is in fact significantly larger than the off-plane anisotropy $\Delta E_{xz} = -0.5$ meV/at (see Fig. 8). Quantitatively, the calculated energy barrier ΔE_{xz} for $\varepsilon_z = 0$ corresponds to a coercive field $H_c = \Delta E_{xz}/M \simeq 5$ T and a blocking temperature $T_B = 3\Delta E_{xz}/k_B \simeq 15$ K. Applying a perpendicular EF from the cluster toward the graphene layer ($\varepsilon_z < 0$) stabilizes the off-plane magnetization direction relative to the in-plane directions. Thus, ΔE_{xz} and ΔE_{yz} increase up to quite significant values, for example $\Delta E_{xz} = 6.2$ meV/at for $\varepsilon_z = -0.75$ V/Å (see Fig. 8). This results in a remarkable EF-induced spin reorientation transition, at a relatively weak $\varepsilon_z = -0.11$ V/Å, from $\vec{M}$ along the x axis to $\vec{M}$ along z axis. At this point, all the orientations of $\vec{M}$ within the xz plane have almost the same energy, and a magnetization reversal process triggered by an external magnetic field becomes barrierless. As already mentioned in the context of Fe_2, the MAE barriers and the stability of the easy magnetization directions $\hat{e}$ and $-\hat{e}$ can be restored at any time by simply removing the external EF.

Although the reversal barrier energy of Co_3 is rather small in the field-free case (structure γ), the in-plane orientation of $\vec{M}$ (x axis) can be further stabilized by applying an outward EF ($\varepsilon_z > 0$). An important enhancement of the MAE is indeed observed in the structure γ for the largest considered fields: $\Delta E_{xz} = 2.3$ meV/at for $\varepsilon_z = 0.75$ V/Å, which is more than a factor 4 larger than in the field-free case [see Fig. 8(a)]. The stability of the in-plane magnetization direction is further enhanced if we take into account the changes in the MAE resulting from the field-induced structural transition from γ to β at $\varepsilon_z = 0.27$ V/Å. This change in the adsorption geometry is accompanied by a qualitative change in the nature of the whole MAE landscape: from an easy x axis and a hard yz plane in the configuration γ ($\Delta E_{xz} < 0$ and $\Delta E_{yz} \simeq 0$) to an easy xy plane and a hard z axis in the configuration β ($\Delta E_{xz} < 0$ and $\Delta E_{xy} \simeq 0$).

The overall trend of decreasing ΔE_{xz} with increasing ε_z, which is observed in the configuration γ of Co_3, is qualitatively similar to the behavior found for the Co atom and dimer on graphene (compare Figs. 5, 6, and 8). This can be correlated with a corresponding decrease of the orbital-moment anisotropy ΔL_{zx} with increasing ε_z, as shown in Fig. 8(b). Moreover, notice that ΔL_{zx} changes sign nearly at the same $\varepsilon_z = -0.1$ V/Å where the spin-reorientation transition occurs. This is consistent with the perturbation-theory analysis reported in Ref. [65] and with the second-order-like angular dependence of the ground-state energy $\Delta E(\theta) = E(\theta) - E_z$ shown in the inset of Fig. 8(a).

The approximate proportionality between ΔE_{xz} and ΔL_{zx} of small Co clusters on graphene (Figs. 5, 6, and 8) contrasts with the behavior found in the case of Fe clusters, whose easy axes do not coincide with the directions yielding the largest orbital moment (see Table I). It is therefore interesting to analyze the microscopic origin of these differences by comparing the corresponding local electronic structures. As an example, Fig. 9 shows the spin-polarized local densities of states $\rho_\sigma(\varepsilon)$ of Fe_3 and Co_3 having the β adsorption configuration. In both cases, one observes large valence-electron densities, which are dominated by the $3d$-orbital contributions, and which present typical FM

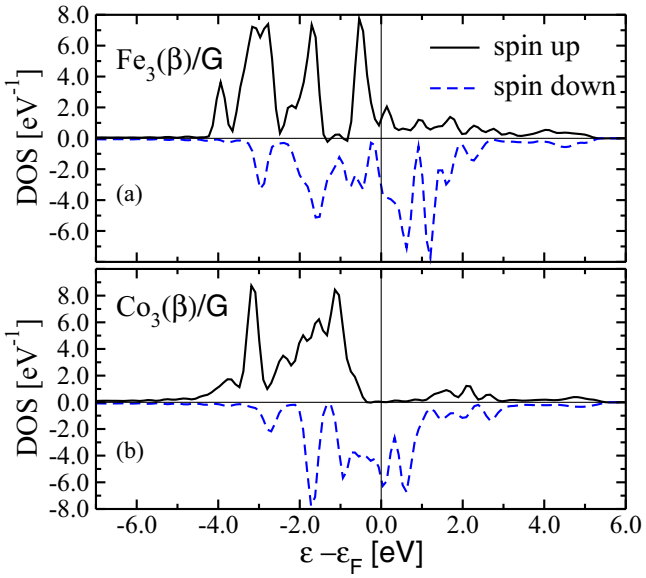

FIG. 9. Spin-polarized density of Kohn-Sham electronic states (DOS) $\rho_\sigma(\varepsilon)$ of Fe_3 and Co_3 on graphene in the adsorption configuration β. See also Fig. 3. The single-particle energy ε is referred to the Fermi energy ε_F.

exchange splittings between majority- and minority-spin states. Notice that the exchange splittings are very similar ($\Delta\varepsilon_X \simeq 1.3-1.7$ eV), whereas the $3d$ bands are somewhat narrower in the case of Co. The most significant differences are found in the behavior at and around the Fermi energy ε_F. In Fe_3 one observes that both $\rho_\uparrow(\varepsilon_F)$ and $\rho_\downarrow(\varepsilon_F)$ are nonvanishing. This implies that both occupied and unoccupied states with different spin projections are present at the same or very similar energies. Consequently, spin-orbit transitions involving spin flips as well as higher-order perturbation contributions to the MAE of Fe clusters on graphene should not be negligible. The working hypothesis of Ref. [65] is not given, and therefore a proportionality between ΔE_{xz} and ΔL_{zx} need not be expected. In contrast, in Co_3 we find a 100% spin polarization at ε_F and an important gap, about 1 eV, between the highest peak in the majority-spin DOS and the lowest unoccupied minority-spin states at ε_F. In this case, Bruno's relation between the energy and orbital-moment anisotropies should apply, as it does, at least qualitatively [65]. Thus, in small Co clusters on graphene, the easy axis can be regarded as the magnetization direction yielding the largest $\langle\vec{L}\rangle$.

IV. CONCLUSION

The main purpose of this work has been to explore the possibilities of controlling the structure and magnetism of transition-metal surface nanostructures by means of static electric fields. Toward that end, first-principles calculations based on density-functional theory have been performed by considering small Fe_N and Co_N clusters on graphene ($N \leqslant 3$) as particularly relevant examples of fundamental and technological interest. The study revealed a variety of remarkable electric and magnetic behaviors that defy easy generalizations. An exceptionally broad range of magnetic

anisotropy energies ΔE has been observed, which goes from $\Delta E \simeq 0.5-1$ meV/at in low-symmetry situations (e.g., Fe_2/G) to colossal values such as $\Delta E \simeq 45$ meV/at in high-symmetry adsorption configurations (e.g., Co_2/G). Moreover, we have shown that ΔE can be tuned by varying the strength and direction of the electric field ε_z. In some cases (e.g., Co_3/G), it is even possible to induce a spin-reorientation transition (i.e., to change the direction of the easy axis) or to almost completely erase the magnetic anisotropy barriers by applying the appropriate ε_z. This should make it possible to reversibly control the coercive field H_c and the blocking temperature T_B of the nanostructures. An EF ε_z could therefore be used, for example, to reduce H_c and thus facilitate the magnetization reversal during the writing process, knowing that the original stability of the magnetization direction (T_B) is restored once ε_z is removed.

In the case of dimers and trimers, one finds extremely interesting adsorption configurations, in which the small clusters stand perpendicular or nearly perpendicular to the graphene layer, thus eluding the intuitive notion of maximal cluster-surface coordination. In addition to the optimal equilibrium structure, one finds a few other metastable geometries (i.e., local minima in the binding-energy surface). These nanostructures show an important structural dependence of the permanent (zero field) dipole moment, which is at the origin of profound, mostly discontinuous changes in the adsorption morphology as a function of the applied ε_z. In addition to the fundamental importance of electric-field-induced structural changes, it is interesting to note that these effects provide a further means of manipulating the magnetic behavior. Indeed, our study shows that the structural rearrangements are accompanied by spin-reorientation transitions and changes in the energy barriers, since the MAE landscape depends critically on the underlying geometry.

The rich diversity of results reported in the present contribution opens a number of interesting perspectives. For example, it would be most worthwhile to follow the electric-field dependence of the magnetic properties of small Fe_N and Co_N clusters on graphene as a function of cluster size and coverage. Further remarkable magnetoelectric phenomena are indeed expected in the complete submonolayer and ultrathin film regime, particularly as the MAE per atom tends to decrease with increasing system size, and as the graphene-mediated interactions among the clusters start to develop. Another important subject is the magnetic consequences of modifications of the graphene electronic structure, which result from hybridizations with different supports. Experiments have already shown that the nature of the substrate is often non-negligible [5,19]. Therefore, understanding the properties of magnetic clusters deposited on graphene-capped surfaces seems challenging. In view of the reported results and the perspectives they open, one concludes that the electric-field manipulation and control of the magnetic properties of small TM clusters on graphene emerges as an extremely promising field of fundamental and technological research from both experimental and theoretical perspectives.

ACKNOWLEDGMENTS

Helpful discussions with K. Türschmann and P. Ruiz-Díaz are gratefully acknowledged. This work has been supported in part by the Deutsche Forschungsgemeinschaft, by the DAAD-CONACyT research program PROALMEX, and by the CONACyT Grant No. 256132. Computer resources were provided by the IT Service Center of the University of Kassel and by the Center for Scientific Computing of the University of Frankfurt. J.D.D. also acknowledges technical support by J. Rentería and J. C. Sánchez.

[1] A. Fert, V. Cros, and J. Sampaio, Nat. Nanotechnol. **8**, 152 (2013); S. S. Parkin, M. Hayashi, and L. Thomas, Science **320**, 190 (2008); N. Romming, Ch. Hanneken, M. Menzel, J. E. Bickel, B. Wolter, K. von Bergmann, A. Kubetzka, and R. Wiesendanger, *ibid.* **341**, 636 (2013).

[2] A. A. Khajetoorians, M. Valentyuk, M. Steinbrecher, T. Schlenk, A. Shick, J. Kolorenc, A. I. Lichtenstein, T. O. Wehling, R. Wiesendanger, and J. Wiebe, Nat. Nanotechnol. **10**, 958 (2015).

[3] K. von Bergmann, Science **349**, 234 (2015).

[4] G. Ju, Y. Peng, E. K. C. Chang, Y. Ding, A. Q. Wu, X. Zhu, Y. Kubota, T. J. Klemmer, H. Amini, L. Gao, Z. Fan, T. Rausch, P. Subedi, M. Ma, S. Kalarickal, C. J. Rea, D. V. Dimitrov, P.-W. Huang, K. Wang, X. Chen, C. Peng, W. Chen, J. W. Dykes, M. A. Seigler, E. C. Gage, R. Chantrell, and J.-U. Thiele, IEEE Trans. Magn. **51**, 3201709 (2015).

[5] F. Donati, Q. Dubout, G. Autes, F. Patthey, F. Calleja, P. Gambardella, O. V. Yazyev, and H. Brune, Phys. Rev. Lett. **111**, 236801 (2013).

[6] A. A. Khajetoorians, M. Steinbrecher, M. Ternes, M. Bouhassoune, M. dos Santos Dias, S. Lounis, J. Wiebe, and R. Wiesendanger, Nat. Commun. **7**, 10620 (2016).

[7] M. Tsujikawa, S. Haraguchi, T. Oda, Y. Miura, and M. Shirai, J. Appl. Phys. **109**, 07C107 (2011); M. Tsujikawa, S. Haraguchi, and T. Oda, *ibid.* **111**, 083910 (2012).

[8] P. Gambardella, S. Rusponi, M. Veronese, S. S. Dhesi, C. Grazioli, A. Dallmeyer, I. Cabria, R. Zeller, P. H. Dederichs, K. Kern, C. Carbone, and H. Brune, Science **300**, 1130 (2003).

[9] R. Félix-medina, J. Dorantes-Dávila, and G. M. Pastor, New J. Phys. **4**, 100 (2002).

[10] P. Błoński and J. Hafner, J. Phys.: Condens. Matter **21**, 426001 (2009); P. Błoński, A. Lehnert, S. Dennler, S. Rusponi, M. Etzkorn, G. Moulas, P. Bencok, P. Gambardella, H. Brune, and J. Hafner, Phys. Rev. B **81**, 104426 (2010).

[11] M. Muñoz-Navia, J. Dorantes-Dávila, D. Zitoun, C. Amiens, B. Chaudret, M.-J. Casanove, P. Lecante, N. Jaouen, A. Rogalev, M. Respaud, and G. M. Pastor, Faraday Discuss. **138**, 181 (2008).

[12] N. N. Negulyaev, J. Dorantes-Dávila, L. Niebergall, L. Juárez-Reyes, G. M. Pastor, and V. S. Stepanyuk, Phys. Rev. B **87**, 054425 (2013).

[13] T. Balashov, T. Schuh, A. F. Takács, A. Ernst, S. Ostanin, J. Henk, I. Mertig, P. Bruno, T. Miyamachi, S. Suga, and W. Wulfhekel, Phys. Rev. Lett. **102**, 257203 (2009).

[14] Zero-point spin fluctuations have also been reported to reduce the effective energy barrier resulting from the magnetic anisotropy of 3*d* and 4*d* TM adatoms on Cu and Ag surfaces. See J. Ibañez-Azpiroz, M. dos Santos Dias, S. Blügel, and S. Lounis, Nano Lett. **16**, 4305 (2016).

[15] I. Bergenti, V. Dediu, M. Prezioso, and A. Riminucci, Philos. Trans. Soc. A **369**, 3054 (2011).

[16] T. Eelbo, M. Waśniowska, P. Thakur, M. Gyamfi, B. Sachs, T. O. Wehling, S. Forti, U. Starke, C. Tieg, A. I. Lichtenstein, and R. Wiesendanger, Phys. Rev. Lett. **110**, 136804 (2013); T. Eelbo, M. Waśniowska, M. Gyamfi, S. Forti, U. Starke, and R. Wiesendanger, Phys. Rev. B **87**, 205443 (2013).

[17] I. G. Rau, S. Baumann, S. Rusponi, F. Donati, S. Stepanow, L. Gragnaniello, J. Dreiser, C. Piamonteze, F. Nolting, S. Gangopadhyay, O. R. Albertini, R. M. Macfarlane, C. P. Lutz, B. A. Jones, P. Gambardella, A. J. Heinrich, and H. Brune, Science **344**, 988 (2014).

[18] C. Antoniak, M. Gruner, M. Spasova, A. Trunova, F. M. Römer, A. Warland, B. Krumme, K. Fauth, Sh. Sun, P. Entel, M. Farle, and H. Wende, Nat. Commun. **2**, 528 (2011).

[19] F. Donati, L. Gragnaniello, A. Cavallin, F. D. Natterer, Q. Dubout, M. Pivetta, F. Patthey, J. Dreiser, C. Piamonteze, S. Rusponi, and H. Brune, Phys. Rev. Lett. **113**, 177201 (2014).

[20] Q. Dubout, F. Donati, C. Wäckerlin, F. Calleja, M. Etzkorn, A. Lehnert, L. Claude, P. Gambardella, and H. Brune, Phys. Rev. Lett. **114**, 106807 (2015); S. M. Valvidares, J. Dorantes-Dávila, H. Isern, S. Ferrer, and G. M. Pastor, Phys. Rev. B **81**, 024415 (2010).

[21] H. Ohno, D. Chiba, F. Matsukura, T. Omiya, E. Abe, T. Dietl1, Y. Ohno, and K. Ohtani, Nature (London) **408**, 944 (2000).

[22] F. Matsukura, Y. Tokura, and H. Ohno, Nat. Nanotechnol. **10**, 209 (2015).

[23] L. J. Li, E. C. T. O'Farrell, K. P. Loh, G. Eda, B. Özyilmaz and A. H. Castro Neto, Nature (London) **529**, 185 (2016).

[24] Y. Fan, X. Kou, P. Upadhyaya, Q. Shao, L. Pan, M. Lang, X. Che, J. Tang, M. Montazeri, K. Murata, L.-T. Chang, M. Akyol, G. Yu, T. Nie, K. L. Wong, J. Liu, Y. Wang, Y. Tserkovnyak, and K. L. Wang, Nat. Nanotechnol. **11**, 352 (2016).

[25] F. Ibrahim, H. X. Yang, A. Hallal, B. Dieny, and M. Chshiev, Phys. Rev. B **93**, 014429 (2016).

[26] P. Ruiz-Díaz, T. R. Dasa, and V. S. Stepanyuk, Phys. Rev. Lett. **110**, 267203 (2013).

[27] M. Fechner, P. Zahn, S. Ostanin, M. Bibes, and I. Mertig, Phys. Rev. Lett. **108**, 197206 (2012).

[28] R. E. George, J. P. Edwards, and A. Ardavan, Phys. Rev. Lett. **110**, 027601 (2013).

[29] S. A. Wolf, D. D. Awschalom, R. A. Buhrman, J. M. Daughton, S. von Molnár, M. L. Roukes, A. Y. Chtchelkanova, and D. M. Treger, Science **249**, 1488 (2001).

[30] I. M. Miron, K. Garello, G. Gaudin, P.-J. Zermatten, M. V. Costache, S. Auffret, S. Bandiera, B. Rodmacq, A. Schuhl, and P. Gambardella, Nature (London) **476**, 189 (2011).

[31] J. Hu and R. Wu, Phys. Rev. Lett. **110**, 097202 (2013).

[32] D. Preziosi, M. Alexe, D. Hesse, and M. Salluzzo, Phys. Rev. Lett. **115**, 157401 (2015).

[33] K. Nakamura, R. Shimabukuro, Y. Fujiwara, T. Akiyama, T. Ito, and A. J. Freeman, Phys. Rev. Lett. **102**, 187201 (2009); K. Nakamura, R. Shimabukuro, T. Akiyama, T. Ito, and A. J. Freeman, Phys. Rev. B **80**, 172402 (2009).

[34] M. Tsujikawa and T. Oda, Phys. Rev. Lett. **102**, 247203 (2009); S. Subkow and M. Fähnle, Phys. Rev. B **84**, 054443 (2011); T. R. Dasa, P. A. Ignatiev, and V. S. Stepanyuk, *ibid.* **85**, 205447 (2012).

[35] N. N. Negulyaev, V. S. Stepanyuk, W. Hergert, and J. Kirschner, Phys. Rev. Lett. **106**, 037202 (2011).

[36] T. R. Dasa, P. Ruiz-Díaz, O. O. Brovko, and V. S. Stepanyuk, Phys. Rev. B **88**, 104409 (2013).

[37] E. Torun, H. Sahin, C. Bacaksiz, R. T. Senger, and F. M. Peeters, Phys. Rev. B **92**, 104407 (2015).

[38] S. Zhang, Y. Zhao, X. Xiao, Y. Wu, S. Rizwan, L. Yang, P. Li, J. Wang, M. Zhu, H. Zhang, X. Jin, and X. Han, Sci. Rep. **4**, 3727 (2014).

[39] X. Xue, Z. Zhou, B. Peng, M. Zhu, Y. Zhang, W. Ren, T. Ren, Xi Yang, T. Nan, N. X. Sun, and M. Liu, Sci. Rep. **5**, 16480 (2015).

[40] A. Sonntag, J. Hermenau, A. Schlenhoff, J. Friedlein, S. Krause, and R. Wiesendanger, Phys. Rev. Lett. **112**, 017204 (2014).

[41] J. Stöhr, H. C. Siegmann, A. Kashuba, and S. J. Gamble, Appl. Phys. Lett. **94**, 072504 (2009).

[42] W. Töws and G. M. Pastor, Phys. Rev. Lett. **115**, 217204 (2015), and references therein.

[43] E. Beaurepaire, J.-C. Merle, A. Daunois, and J.-Y. Bigot, Phys. Rev. Lett. **76**, 4250 (1996).

[44] T. Maruyama, Y. Shiota, T. Nozaki, K. Ohta, N. Toda, M. Mizuguchi, A. A. Tulapurkar, T. Shinjo, M. Shiraishi, S. Mizukami, Y. Ando, and Y. Suzuki, Nat. Nanotechnol. **4**, 158 (2009).

[45] T. Nozaki, Y. Shiota, M. Shiraishi, T. Shinjo, and Y. Suzuki, Appl. Phys. Lett. **96**, 022506 (2010).

[46] S.-S. Ha, N.-H. Kim, S. Lee, C.-Y. You, Y. Shiota, T. Maruyama, T. Nozaki, and Y. Suzuki, Appl. Phys. Lett. **96**, 142512 (2010).

[47] M. Endo, S. Kanai, S. Ikeda, F. Matsukura, and H. Ohno, Appl. Phys. Lett. **96**, 212503 (2010).

[48] Z. Wang, Y. Yang, R. Viswan, J. Li, and D. Viehland, Appl. Phys. Lett. **99**, 043110 (2011).

[49] Y. Suzuki, H. Kubota, A. Tulapurkar, and T. Nozaki, Philos. Trans. R. Soc. A **369**, 3658 (2011).

[50] K. Kita, D. W. Abraham, M. J. Gajek, and D. C. Worledge, J. Appl. Phys. **112**, 033919 (2012).

[51] M. Weisheit, S. Fähler, A. Marty, Y. Souche, C. Poinsignon, and D. Givord, Science **315**, 349 (2007).

[52] F. Bonell, S. Murakami, Y. Shiota, T. Nozaki, T. Shinjo, and Y. Suzuki, Appl. Phys. Lett. **98**, 232510 (2011).

[53] K. Shimamura, D. Chiba, S. Ono, S. Fukami, N. Ishiwata, M. Kawaguchi, K. Kobayashi, and T. Ono, Appl. Phys. Lett. **100**, 122402 (2012).

[54] N. Tournerie, A. P. Engelhardt, F. Maroun, and P. Allongue, Phys. Rev. B **86**, 104434 (2012).

[55] T. J. Zhou, S. H. Leong, Z. M. Yuan, S. B. Hu, C. L. Ong, and B. Liu, Appl. Phys. Lett. **96**, 012506 (2010).

[56] G. Kresse and J. Hafner, Phys. Rev. B **47**, 558 (1993); G. Kresse and J. Furthmüller, *ibid.* **54**, 11169 (1996).

[57] P. E. Blöchl, Phys. Rev. B **50**, 17953 (1994); G. Kresse and D. Joubert, *ibid.* **59**, 1758 (1999).

[58] J. P. Perdew and Y. Wang, Phys. Rev. B **45**, 13244 (1992).

[59] H. Johll, H. C. Kang, and E. S. Tok, Phys. Rev. B **79**, 245416 (2009).

[60] H. Johll, J. Wu, S. W. Ong, H. Ch. Kang, and E. S. Tok, Phys. Rev. B **83**, 205408 (2011).

[61] X. Liu, C.-Z. Wang, H.-Q. Lin, M. Hupalo, P. A. Thiel, K.-M. Ho, and M. C. Tringides, Phys. Rev. B **90**, 155444 (2014).

[62] Systematic tests on the convergence of the total energy of Fe and Co atoms on graphene have been performed in Ref. [59]. Thus, Johll *et al.* concluded that a 4×4 supercell with a vertical size $a_z = 12.4$ Å, a cutoff energy $E_{\max} \simeq 400-550$ eV, and an $8 \times 8 \times 1$ Monkhorst mesh are adequate (see also Ref. [60]). Liu *et al.* (Ref. [61]) considered a 6×6 supercell with $a_z = 15$ Å, $E_{\max} = 600$ eV, and a $4 \times 4 \times 1$ Monkhorst mesh. Our technical parameters (6×6 supercell with $a_z = 16$ Å, $E_{\max} = 500$ eV with tests at 750 eV, and a $6 \times 6 \times 1$ Monkhorst mesh) are similar to or better than in previous studies. Any further numerical fluctuations are estimated to be of the order 10 meV/at, which are clearly smaller than the energy differences between different adsorption configurations, of the order of 100–300 meV/at, as discussed in the main text. Furthermore, notice that larger values of a_z are advantageous, since this corresponds to the symmetry of the cluster-on-surface geometry, and in order to avoid spurious couplings between the electronic density and the dipole layer, which is the source of the applied EF.

[63] C. D. Porter and D. Stroud, Phys. Rev. B **85**, 235452 (2012).

[64] G. Nicolas, J. Dorantes-Dávila, and G. M. Pastor, Phys. Rev. B **74**, 014415 (2006).

[65] P. Bruno, *Magnetismus von Festkörpern und Grenzflächen*, edited by P. H. Dederichs, P. Grünberg, and W. Zinn (KFA, Jülich, 1993), Chap. 24.

[66] T. O. Wehling, A. V. Balatsky, M. I. Katsnelson, A. I. Lichtenstein, and A. Rosch, Phys. Rev. B **81**, 115427 (2010).

[67] It should be noted that in addition to the self-consistency issue, there are other, more technical differences between the present calculations and those reported in Ref. [37]. In our case, we solve the KS equations in the GGA to exchange and correlation, including dipole corrections, using a 72-atom supercell, and requiring an energy accuracy of 10^{-7} eV/at for each considered direction of the magnetization. In Ref. [37], the DFT + D2 method is used, which incorporates long-range dispersion forces, and the KS equations are solved in a supercell containing 32 atoms, using also the GGA but excluding SO interactions, and requiring an energy accuracy of 10^{-5} eV/at. The MAE is then obtained by treating the SO interactions to first order in the force-theorem approximation.